TETHERED-TUGS FOR ACTIVE DEBRIS REMOVAL: MICROGRAVITY EXPERIMENTAL VALIDATION OF DYNAMICS AND CONTROL

R. Benvenuto[(1)], M. Lavagna[(1)], P. Lunghi[(1)], V. Pesce[(1)], A. Bellanca[(1)], S. Rafano[(1)],

A. Delahaye[(2)], L. Pfeiffer[(3)]

[(1)] *Politecnico di Milano, Department of Aerospace Science and Technologies, Via La Masa 34, 20156 Milano, Italy*

Email: michelle.lavagna@polimi.it

[(2)] *QinetiQ Space nv, Hogenakkerhoekstraat 9, 9150 Kruibeke, Belgium*

Email: ann.delahaye@qinetiq.be

[(3)] *ESTEC, European Space Agency, Keplerlaan 1, 2201 AZ Noordwijk, The Netherlands*

Email: lukas.pfeiffer@esa.int

ABSTRACT

The SatLeash experiment, flown on-board Novespace's Zero-G aircraft in the 65th ESA Parabolic Flight Campaign in October/November 2016, as a part of ESA Education Fly Your Thesis! Programme, investigated the dynamics and control of tow-tethers, for space transportation. Towing objects in space through a tether has become a common concept for many missions such as active debris removal, satellite servicing and even asteroids retrieval. The team exploited a multibody dynamics simulator to describe tethered-satellite-systems dynamics and synthetize their control. The in-flight experiment focused on validating the adopted models and verifying the implemented control laws. The paper briefly introduces firstly the models set up together with the adopted control law, gives the simulations' rationale, describes the flight experiment design and integration, to secondly focus the attention on the experimental campaign data and data post-processing. The validation process is, then, explained and preliminary results are discussed.

1 INTRODUCTION

1.1 Scientific background

Since the beginning of space era more than 6000 objects (ca. 7000 tons of material) have been launched into Earth orbit and today less than 1000 are still operational satellites. The rest is composing the so-called *space debris* population, comprised of de-activated and dead satellites, upper stages of rocket carriers and smaller pieces, products of fragmentations and collisions. All these objects are uncontrolled and pose a serious risk for space exploitation sustainability and safety of future orbital operations. The need of active remediation has been advocated more and more in the last few years by the scientific community, to avoid future collision hazard and preserve the space environment. Recent studies run by NASA [1] and ESA [2] revealed that the environment can be stabilized if objects in the order of 5 to 10 per year are removed from space. In order for ADR to be the most effective in the collision occurrence reduction, previous studies showed that it shall target the most massive debris in highly inclined orbits.

Active debris removal (ADR) focuses on designing and making operational mechanisms placed on board an active spacecraft that can rendezvous with and grapple an inert and tumbling target, to eventually change its path. Most of the proposed ADR technologies are based on distance capturing and establishing elastic flexible connections with debris: these techniques are inspired by methods exploited on Earth since ancient history for fishing and hunting. No matter what the capture technique is, the composite spacecraft-tether-debris system is the so-called tethered space tug: after capture, the two objects are connected by the tethered-net flexible link, the motion of the system being excited by the active spacecraft propulsion system. In particular, tether being a long cable, made of long strands of high strength fibres. The tug concept is illustrated in Figure 1.

The tethered tug was firstly studied by Aslanov and Yudintsev ([3], [4]) and Jasper and Schaub ([5], [6]) who independently studied different control techniques using a simplified simulation environment. In particular Jasper and Schaub studied input shaping techniques of the thrust profile to cut off the tethered-system's first modes frequencies, significantly reducing the bounce back and tether oscillations.

Proc. 7th European Conference on Space Debris, Darmstadt, Germany, 18–21 April 2017, published by the ESA Space Debris Office
Ed. T. Flohrer & F. Schmitz, (http://spacedebris2017.sdo.esoc.esa.int, June 2017)

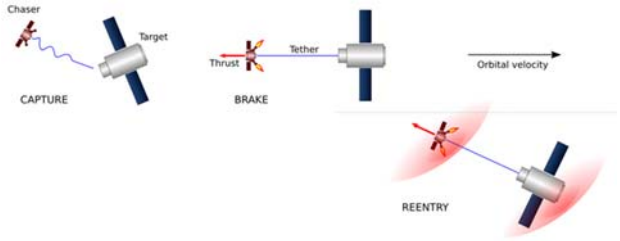

Figure 1 - Tethered-Tug concept

Space tugs open new challenges for guidance navigation and control (GNC) design. The chaser's GNC system is required to robustly perform de-orbiting operations while controlling a complex system and damping vibrations of flexible elements and connections, avoiding instability, collisions, and tether entanglement. Adapted control techniques and active vibration damping need to be investigated to allow carrying out operations safely and autonomously and it is this area that the SatLeash project falls into.

1.2 Microgravity and parabolic flights

Due to flexibility, zero gravity environment and coupled end-bodies dynamics, tethered-systems undergo a complicated set of three-dimensional librations and vibrations. Therefore, it is necessary to study their three-dimensional behaviour in microgravity and to this end parabolic flights are the most suited facilities for both time-span and available test area, among the ones available on ground.

On the surface of our planet, everything is affected by gravity. The only way to counteract the effect of gravity on an object is to accelerate it with an acceleration equal to the one induced by gravity itself: this status is familiarly known as free-fall. Onboard the Novespace's Airbus "Zero G", microgravity is obtained with a controlled free falling manoeuvre of the aircraft along a parabolic trajectory. During the experimental campaign, 3 flights are scheduled, each one including 30 parabolas. Each manoeuvre starts with a 50 degrees climb when the gravity level on board is higher than normal, a situation called *hyper gravity*. Before the peak of the parabola, engines are put in idle making the aircraft enter in free-fall state. The *A310* "Zero G" can guarantee 22 seconds in weightlessness level. During this phase, the aircraft performs a slow pitching manoeuvre in order to point its nose downward. Then, a 45 degrees' descent is started: a second period of *hyper gravity* is experienced exiting the parabolic path when the normal horizontal flight attitude is regained. In Figure 2, the above described parabolic flight sequence is represented.

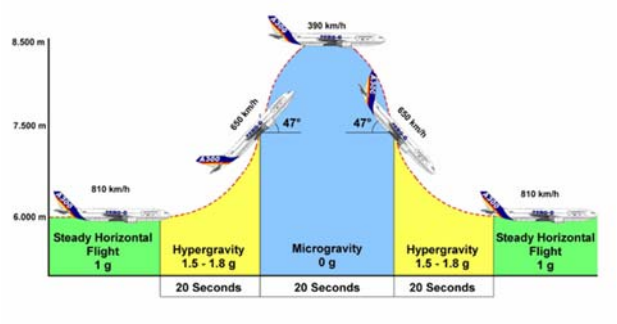

Figure 2 – Parabolic flight sequence

1.3 Objectives of the project

The Fly Your Thesis! programme of the European Space Agency's Education Office offers university students the opportunity to conduct their scientific experiments in microgravity conditions during a parabolic flight campaign. In this framework, the PoliTethers team, from Politecnico di Milano, Department of Aerospace Science and Technologies (PoliMi-DAER), was selected to fly an experiment on-board Novespace's Zero-G aircraft in the 65th ESA Parabolic Flight Campaign in October/November 2016.

The *SatLeash* experiment[1], whose logo is depicted in Figure 3, investigated the dynamics and control of tow-tethers, for space transportation.

Figure 3 – SatLeash Logo

One of the most common critical modes that may arise during towing operations is the bounce-back effects. Whenever thrust is shut down, the tether slackens and the residual tension accelerates the two objects towards each other, increasing the risk of collision. After this mode, the control recovery is difficult and not always possible. The tether may entangle on the target or the chaser itself leading to its breakage. Control methods based on shaping the thrust profile through a wave-based controller, using tension feedback, proved to be

[1] www.SatLeash.it

effective in simulation to stabilize the system during tensioning and release phases. Validated simulation tools describing tethered-tugs dynamics, and their stabilization via control laws, are considered of primary importance to design future missions. To this end, the team exploited a multibody dynamics simulator to describe tethered-satellite-systems dynamics and synthetize their control. The in-flight experiment focused on validating the adopted models and verifying the implemented control laws for the chaser thrust modulation. A reduced-scale tethered floating test bed flew equipped with a stereovision system to reconstruct its 3D trajectory and acceleration sensors to measure g-jitter. Different tether stiffnesses were tested as well as control schemes to verify their effectiveness in stabilizing the system, reducing whiplash and bouncing-back effects. The set-up architecture is presented in Figure 4 and it will be detailed along the paper.

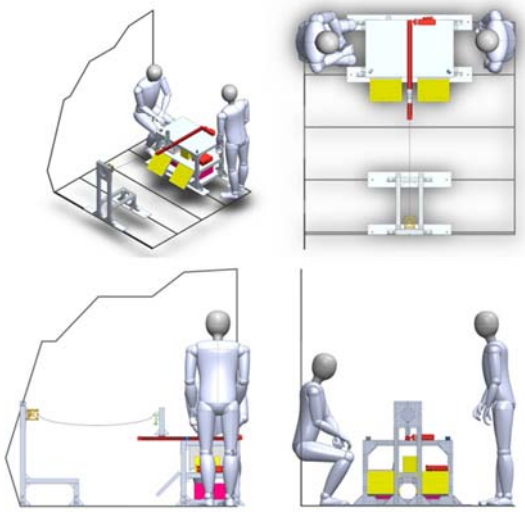

Figure 4 – Experimental set-up architecture

The flight campaign run successfully and data from more than 65 parabolas over 90 have been acquired. The experiment confirmed the effectiveness of the proposed control strategy. Interesting μ-g effects have been observed on the tether tension law which differs from the 1-g scenario.

Section 2 introduces the implemented dynamics models together with the adopted control laws. Section 3 describes the flight experiment design and integration, as well as the experimental campaign, data post-processing and test cases results. Conclusions are finally drawn in section 4.

2 TETHER DYNAMICS AND CONTROL

2.1 Multibody Dynamics Simulator

At PoliMi-DAER, the problem has been deeply analysed to simulate at the best the phenomenon: to this end, the team has developed a dedicated multibody dynamics simulation tool to describe the tethered-satellite-systems dynamics and design their control. The tool has been entirely developed in Matlab/Simulink. The multibody constrained dynamics have been represented through a discretized viscoelastic model for the flexible components, and taking into account the six degrees of freedom end-satellites. The system dynamics can be investigated in any gravity/acceleration field, spanning from deep space conditions, orbital conditions, ground conditions and parabolic flight conditions. The software has been verified and validated through benchmarking with analytical and on ground experimental results. The parabolic flight test campaign is now expected to provide the ultimate validation in microgravity.

The analysis of tethered systems is performed using discrete-mass representations or lumped parameters methods. Flexible systems discrete-mass representations are used frequently ([3], [4], [5], [6], [7], [8]): they are able to model higher-order tether modes while capturing end-bodies motion on both ends of the tether. The dynamics behaviour can be adequately described, obtaining an approximate solution for tether flexing and whipping but allowing a fast-computational environment, particularly adapted to synthetize and test guidance and control laws. Conceptual representation of lumped models is presented in Figure 5: it is remarked that while the first model is non-linear and only able to describe axial stiffness, the second is linear and can also account for bending and torsion.

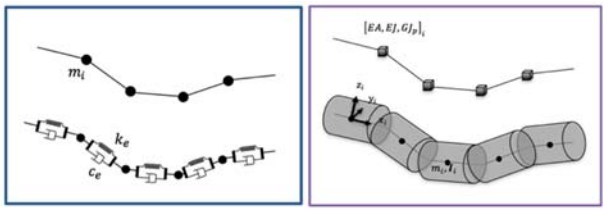

Figure 5 - Lumped models conceptual representation

Moreover, these models allow describing the system parametrically, to treat different configurations and include different viscoelastic laws: for example, two laws are implemented in the simulator for material tension.

The first is the linear Kelvin-Voigt law:

$$T = \begin{cases} -k|x| - d\dot{x} & if\ x > 0 \\ 0 & if\ x \leq 0 \end{cases} \quad (1)$$

where

- k and d are the elastic and viscous parameters between two discretization nodes
- x is the elongation and $\dot{x}$ is the relative velocity

The second is the non-linear Hunt-Crossley law:

$$T = \begin{cases} -k|x|^n - d|x|^n\dot{x} & if\ x > 0 \\ 0 & if\ x \leq 0 \end{cases} \quad (2)$$

These systems and their equations of motion, as well as their control, have already been treated in detail in previous publications ([9], [10], [11]) and are only mentioned here. In particular, the differences between the two models in terms of hysteresis cycle and physical representativeness of coefficients were detailed in [10]. Furthermore, the environment perturbative models (i.e. atmospheric drag and solar pressure) were also derived in [11] for discretized tethered structures.

The discretized model that was used for full-scale dynamics simulations is depicted in Figure 6: the red body represents the controlled chaser, while the blue one is the passive target.

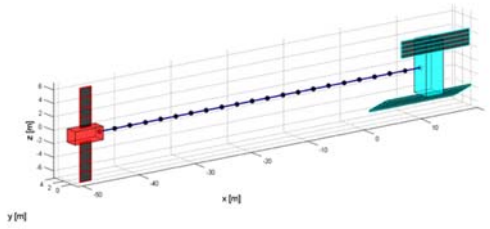

Figure 6 – Multibody model used for full-scale simulations (20 nodes tether discretization)

2.2 Tether control

2.2.1 Critical modes and instabilities

The most common critical modes that may arise during towing operations are whiplashes (sudden rotation of spacecraft occurring right after the towing cable gets stretched) and bounce-back effects (whenever thrust is shut down, the tether slackens and the residual tension accelerates the two objects towards each other, leading to the risk of collision). After these modes, the control recovery is more difficult and not always possible. The tether may entangle on the target or the chaser itself leading to its rupture. A detailed description of these instabilities is reported in [12].

The main requirement for an effective control scheme is then the ability to work both in tensioning phase, avoiding whiplash, and in release phase, avoiding bounce-back. After researching different methods ([9], [11]), the wave-based controller was selected for its straightforward implementation and its robustness face to system uncertainties.

2.2.2 Wave-based controller

The wave-based control (WBC) represents an innovative and robust approach to actively damping vibrations of flexible systems and it was firstly proposed by O'Connor [13] for space tethers applications. Classical frequency shaping techniques require the stabilization of the system prior to their use and the exact knowledge of the system dynamical properties. On the contrary, wave-based control allows to stabilize the system and control the tether tension during pulling with the same controller and without an exact knowledge of system flexibility. Moreover, it is strongly robust to uncertainties. This control strategy fits the problem for the tether elastic behaviour itself. In the wave based idea the axial elastic interaction between chaser and target is interpreted as mechanical waves which travel through the tether from chaser to target and back again from target to chaser. Hence, the actuator motion (i.e. the chaser) is devoted to absorb the returning wave, introducing damping to the flexible system: the effect is similar to have a viscous damper located on the actuator, that absorbs the vibration energy. In its simpler form, in fact, the wave-based controller is implemented as a velocity control strategy, with a proportional law between the tether tension and the damping velocity of the actuator, in the form:

$$v = \frac{T}{Z} \quad (3)$$

where Z is an impedance, computed using the estimated target mass and tether stiffness, and T the tension on the tether. The control law resolves in the simple form:

$$v_C(t) = \frac{1}{2}v_R(t) + \frac{1}{2}\left(v_M(t) - \frac{T_M(t)}{Z}\right) \quad (4)$$

where the subscripts stand for Commanded, Reference and Measured. The resulting controller loop is schematized in Figure 7.

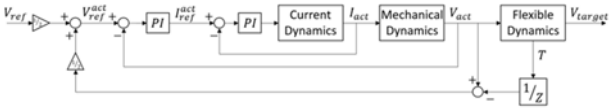

Figure 7 – WB controller

This leads to drive the servomotor of a linear actuator, emulating the chaser pulling action, taking as input the set of required velocities as well as the current slider velocity and the values of tension at the connection between the tether root and the slider part of the actuator as feedback data for the closed loop control system. The tether tension is measured by a load cell, and then amplified and filtered. The reference velocity profile is set as a ramp to simulate the orbital thrusting phase, i.e. a required Delta-V to give to the target.

2.3 Simulations results

By applying the WBC, the full 3D floating system dynamics is reduced to a 2nd order system, as if the chaser was constrained to a skyhook through the controller viscous-damper. This leads to the possibility of substituting the chaser action with a linear actuator responsible of modulating the thrust and emulating the chaser floating body, even if constrained to the airplane. Moreover, in the hypothesis of a tether mass negligible with respect to the target mass, the damping factor introduced by the WBC can be easily estimated as a function of the impedance Z as

$$\xi_{WB} = \frac{\sqrt{K_t m_T}}{2Z} \tag{5}$$

where K_t is the tether stiffness and m_T is the target mass. Now, theoretically Z could be chosen in order to have a ξ_{WB} around 0.7-0.8 (optimum control). This is true for the first phase of pulling when the tether starts slack and gets tensioned. However, being the system non-linear, i.e. notwithstanding compression, it is not the same for the release phase: if ξ_{WB} is lower than 1, the tether collapses and slacken and the tension goes to zero. In other words, in the release phase an overshoot is not acceptable due to the nonlinearity of the tether tension, as described in Equations (1) and (2). The requirement is then to select Z as

$$Z \leq \frac{\sqrt{K_t m_T}}{2} \tag{6}$$

in order to have $\xi_{WB} \geq 1$. Different Z will lead to different transient times but they will not affect the steady-state response. Theoretically, one would want then to select the maximum Z, i.e. critical damping $\xi_{WB} = 1$, to have the lowest transient time. However, due to the limits of the actuator bandwidth and to the uncertainties in the tether stiffness, Z is selected, as a first guess, in order to have a $\xi_{WB} = 2$, considered a sufficient margin to avoid the risk of falling in an underdamped condition. This condition is considered by the following simulations. Furthermore, in the following simulations, a DV of 0.5 m/s is given and the velocity ramp is tuned to limit the drift, due to g-jitter disturbances, at the end of the manoeuvre. Tether and end-body physical parameters are discussed in the next section, where dynamics scaling is presented, and summarized in Table 1.

In Figure 8 and Figure 9, simulation results are presented for the scaled breadboard, respectively for the case without and with active wave-based control, in the ideal case of no perturbations. Results depict a 3D image of the system at the end of the simulation, the actuator velocity profile, the tether tension and the tether length (computed as the relative distance between the floating body and the actuator).

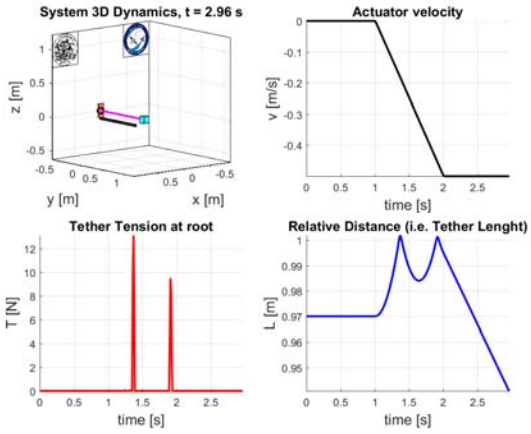

Figure 8 – Simulation results with WBC off

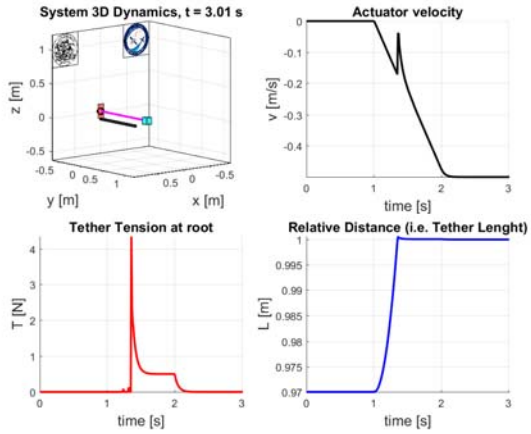

Figure 9 – Simulation results with WBC on

As it is possible to remark, with no control the tether is tensioned through shock loads and slackens in between. The bounce-back at the end of the pulling phase is clearly visible, the two objects approaching each other. On the other hand, when the control is on, the actuator adapts the pulling velocity following the tension detected on the tether, shock loads and tether slack are then avoided and at the end of the pulling phase the relative distance is kept constant, thanks to the gradual release of the pull, as visible in the tension profile.

During a parabola, the acceleration is not perfectly zero but it is kept below 0.05g. This perturbation is called g-jitter. Since the experiment is hinged on the dynamics of floating objects, it is very important to minimize the effects of these disturbance accelerations and to accurately measure it during the parabolic flight in order to consider their effects in the model. In order to assess g-jitter effects on the experiment, acceleration data from real flights, provided by Novespace, have been exploited and given as input to the simulations to support the system design and to finely tune the control parameters. Furthermore, also Coriolis and centrifugal accelerations act on the floating object, their value

depending on the object location and velocity relative to the aircraft rotation axis. It was demonstrated, but it is not reported here, that by knowing the output of an IMU fixed to the aircraft in a known position and of an IMU within the floating object, the accelerations acting on the latter can be derived by difference, knowing the relative position between fixed IMU and floating one, without the need of precisely determine the aircraft rotation axis. These measures were used as input for model validation after the test campaign.

In Figure 10 the same simulation of Figure 9 is repeated, this time including the g-jitter disturbances. This case is closer to what it is expected during flight. The disturbances cause a drift of the target but the control action is still clearly visible and its performances can still be quantified.

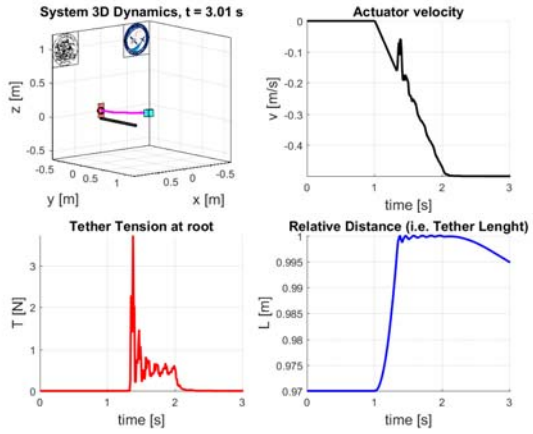

Figure 10 – Simulation results with WBC on and g-jitter disturbance

3 EXPERIMENTAL SET-UP AND TEST CAMPAIGN

3.1 Scaling and dynamics similitude

Using dynamic similitude and scaling methods, the breadboard model was designed as a reduced scale of a reference orbital scenario in order to obtain a complete dynamical representativeness of the full-scale system.

As for any dynamic system, the physical free variables are the forces, the masses, the length and the time; on the other side, the free physical dimensions to be considered for scaling are the mass, the length and the time ([M], [L], [T]). Therefore, according to the Buckingham Pi theorem, a single π non-dimensional term suffices to ensure the dynamics similitude holding; in particular, the $\pi=MLF^{-1}T^{-2}$ must be equal for the model and for the prototype, therefore, from the statement that $\pi_m=\pi_p$ the relationship to scale the forces is obtained:

$$S_F = \frac{S_M S_L}{S_t^2} = S_M S_a \quad (7)$$

being S_i scale factor and i the quantity referring to (Force, Mass, Length, time, acceleration). Equation 7 can then be exploited to derivate, from the experiment, the actual forces on the real scenario, the tether tension being equal to the target mass multiplied by the acceleration given to the system.

Depending on the experiment constraints and driver, actually, the mass, length and time scaling factors can be settled as variables dependent on more convenient quantities. For the current problem, using the Hooke's law and considering the strain scale equal to one (geometric similitude), the scale of tension in the tether can be rewritten as

$$S_F = S_\sigma S_D^2 = S_E S_\varepsilon S_D^2 = S_E S_D^2 \quad (8)$$

where σ is the stress, ε the strain, E the Young's modulus and D the diameter. It is also remarked that setting tether modulus, diameter and length is equivalent to select tether stiffness: it is in fact

$$K_t = \frac{\mathrm{E\,A}}{L} \rightarrow \frac{S_E S_D^2}{S_L} \quad (9)$$

Considering the possibility of modelling the system as a second order system (as explained above), the frequency scale becomes

$$S_\omega = \frac{1}{S_t} = \sqrt{\frac{S_K}{S_M}} \quad (10)$$

Now, by combining Equations 7, 8, 9 and 10, it is possible to choose tether stiffness (i.e. E, D, L) and target mass and to exploit these equations to obtain the scale on all the other geometric, kinematic and dynamic quantities and map them from the experiment data to the in-orbit application.

Finally, once the system dynamics has been scaled, the manoeuvre parameters can be defined in terms of acceleration and ΔV and by consequence manoeuvre time, by combining the above relations with the kinematic relation for velocity as

$$S_v = S_a S_t = \frac{S_a}{S_\omega} = \sqrt{\frac{S_E S_L S_D^2}{S_M}} \quad (11)$$

An example is reported in Table 1, where the Envisat de-orbiting reference scenario was scaled to the test model, considering experimental constraints in term of area size and useable microgravity time (which was reduced to account for drift due to perturbations as explained above). It is possible to remark the scaled manoeuvre represent 33 seconds and a ΔV of 2.8 m/s for the orbital scenario: of course, in orbit the manoeuvre would need to last longer to acquire the needed ΔV, meaning that the experimental case is only describing part of the full manoeuvre.

To confirm these results simulations ran to compare the two outputs. Good matching was found between predicted and simulated data and the scales were confirmed to be respected (force, stress, strain etc.).

Table 1 – Reference Scenario VS. Scaled Model

Parameter	Reference Scenario	Test Model	Scale
Stiffness [N/m]	2.5E3	245.7	10.3
Target Mass [kg]	7815	2.8	2791
Acceleration [m/s2]	8.59E-2	0.3	0.29
Tension [N]	671	0.84	798.7
Frequency [Hz]	9E-2	1.5	6E-2
Stress [Pa]	9.5E7	1.2E5	8E2
Strain [%]	3.8E-3	3.8E-3	1
ΔVelocity [m/s]	2.8	0.6	4.7
Time Manoeuvre [s]	33	2	16.5

3.2 Experimental breadboard

The floating module, tethered connected to the actuator, was similar to a CubeSat with a 12 cm side cubic structure made of thin aluminium plates. It had three floors hosting the IMU, the Raspberry Pi3 and the battery pack, respectively. Lateral plates were added to have uniform lateral surface to locate the markers for stereovision reconstruction (coloured markers were installed on the CubeSat to guarantee relative position, velocity and attitude reconstruction by stereo vision using the two synchronized cameras) and to increase the components protection from the electromagnetic field of the docking mechanism (described below). The bottom plate was made of steel to provide the interface to the electromagnetic docking mechanism. The floors were connected by screws and are mechanically machined to lighten the structure and to create the holes to connect the components by USB cables. The total weight was approximately 2.8 kg. The tether was attached to the upper side of the CubeSat through a cable gland with no end connection. The design is schematized in Figure 11.

The orientation of the rack was driven by the direction of the tether axis: the set-up has been oriented along the Y-axis (pitch axis), in order to minimize the acceleration disturbances on the floating module and maximize the control capability of the actuator. By consequence, all the other components were oriented accordingly. The main rack developed along the aircraft longitudinal axis (X) and the area between the rack and the airplane walls was the free floating zone. The set-up architecture is depicted in *Figure 4*.

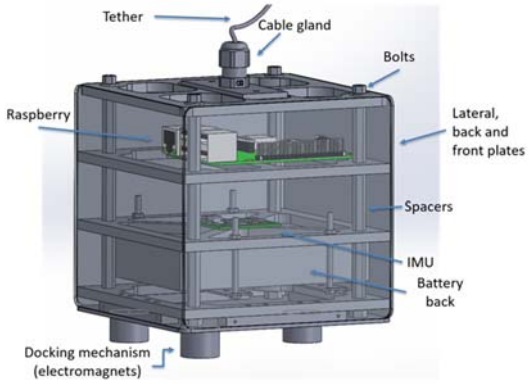

Figure 11 – CubeSat configuration

An illumination system was necessary, dealing with stereovision and high-speed cameras: in order to limit the disturbance due to the illumination system, the lights were oriented along Y, positioned on the floor and activated only during recording time. The floating area was protected by curtains and nets. The black curtains covered the lateral sides of the experimental area. In this way, they provided a uniform and high contrast background, making it easier to visually identify the markers on the cube, but also minimizing the illumination disturbances for the other experiments. The nets were used to protect the operators and the instruments. This guaranteed a confined floating zone, for safety reasons. The high-speed cameras were placed on top of the main rack and a converging configuration was used to optimize the global field of view. Spare parts, spare tethered systems, calibration board and other tools were securely stored in the lower shelf of the main rack behind the illumination system. The secondary rack held the electromagnetic docking mechanism, to fix the cube before the test start. The electromagnets were sized to hold the cube in position during hyper-gravity with an acceptable margin of safety, due to uncertainties in the centre of mass location.

After trading off different linear actuators, considering the requirements of large stroke, low force, high velocity and electromagnetic compatibility with the A310, the FESTO EGC-50-TB-KF-GK was identified as the best solution. It was driven by a servomotor connected through a gear box. The linear stage bandwidth was around 87 Hz, an acceptable value for the experimental application. A 16 bits multistage absolute encoder is embedded into the servomotor and provides the position and velocity measurements as feedback to the controller. By controlling the actuator starting point the initial configuration could present a slack or stretched tether, giving the possibility of conducting different kind of tests and separate tensioning and release phases. A detailed experiment

configuration is shown in Figure 12.

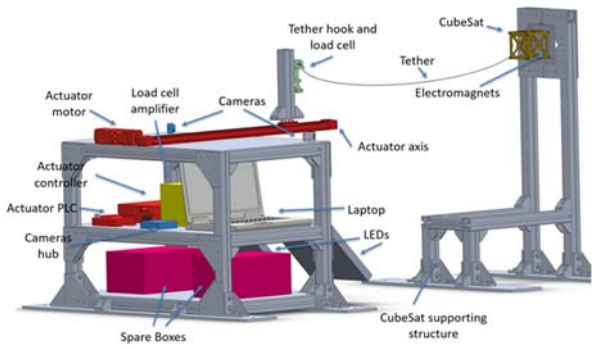

Figure 12 – Experiment configuration

The implementation of a reliable acquisition chain was fundamental for the experiment success: several different sensors were necessary to satisfy all the requirements. Furthermore, a precise synchronization and proper redundancies had to be guaranteed. Two Point Grey Chamaleon 3 stereo cameras (70 fps, 1.3 MPixels) were exploited to reconstruct the position, velocity and attitude of the cube. For dynamics reconstruction purposes, as mentioned above, two high-resolution inertial measurement units (IMU) were installed on the experiment. One was placed on the main rack and the other inside the cube. A precise measure of the tether tension was necessary to provide correct feedback to the wave-based controller: a low-noise FUTEK LSB200 was selected. Finally, the encoder on the actuator motor provided feedback information about position and velocity of the slider. The sensors data acquisition and storage was performed by two Raspberry Pi3 boards (one inside the cube and one on the rack) and by a laptop. The main Raspberry Pi was also the master trigger of the whole experiment and it was connected to the PLC of the linear actuator. In Figure 13, the electronic network is represented in detail.

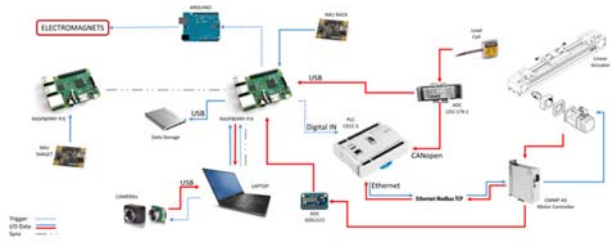

Figure 13 – Electronic network

It is important to remark that tether elasticity and damping are the key parameters playing the fundamental role in its flexible dynamics behaviour. Several materials and tethers' configurations (for example with or without insulation/sheath) were investigated the final test samples. To fully characterize the tethers mechanical properties, including damping, tensile tests and dynamical-mechanical tests ran at PoliMi-DAER laboratories, as well as tests on frictionless table to tune the control parameters. In this facility the 2D motion of the dynamics system could be simulated: even of the tether was affected by gravity and the mass motion was bi-dimensional, ground tests on the low friction table were very useful in selecting the first guess control parameters and calibrate the experiment before flight.

In Figure 14 and Figure 15 the set-up, integrated on-board the A310 *Zero-G* aircraft, and an actual microgravity towing test are shown. During the flight campaign, about 70 out of 90 total parabolas were performed successfully: a huge amount of data was obtained. The whole test campaign, including ground tests allowed to build a database of simulation and experimental data with respect to different environmental conditions, to characterize at best the influence of gravity on the fibres dynamics behaviour. A systematic method was employed to verify and comprehend the different phenomena involved: several configurations were tested in terms of mock-up mass, tether stiffness, manoeuvre and control parameters.

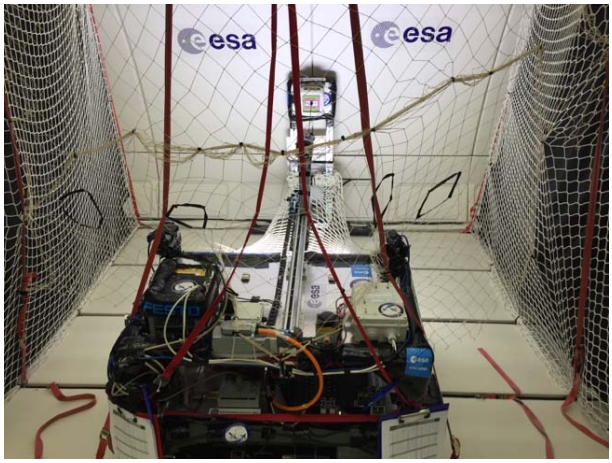

Figure 14 – SatLeash flight configuration

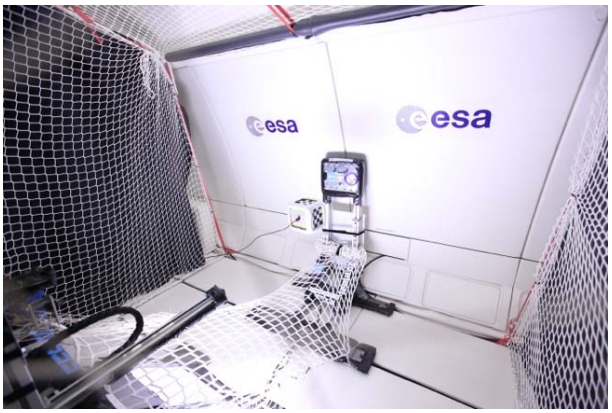

Figure 15 – SatLeash in-flight experiment

3.3 TEST RESULTS

Test results are reported in Figure 16 and Figure 17, respectively for stabilization and release phases. For each case, the relative distance between chaser and target and the tether tension are presented. The test parameters are discussed in Table 2, while the WBC impedance *Z* is depicted in the legend of each figure.

Few preliminary considerations are possible:

- the internal damping of the fibres appears to be lower in microgravity with respect to ground tests, a result that could be explained by a resulting lower friction between the braids;
- the cube drift was lower than expected but could be due to favourable meteorological conditions during the flights;
- a de-noise filter was employed to clean tension data because a higher cut-off frequency was employed to reach better control performances;
- the WBC is very effective and robust and the experimental results match very closely the theoretical previsions.

Table 2: Test case parameters

Parameter	Value
Tether length [m]	0.9
Tether diameter [m]	3E-3
Slack [m]	1.5E-2 (1.67%)
Target Mass [kg]	2.94
Acceleration [m/s2]	0.3
ΔVelocity [m/s]	0.38
Load cell cut-off frequency [Hz]	9.8

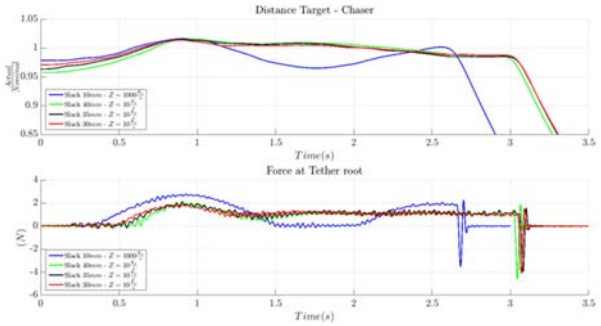

Figure 16 – Stabilization Phase: relative distance and tether tension for different tether slacks

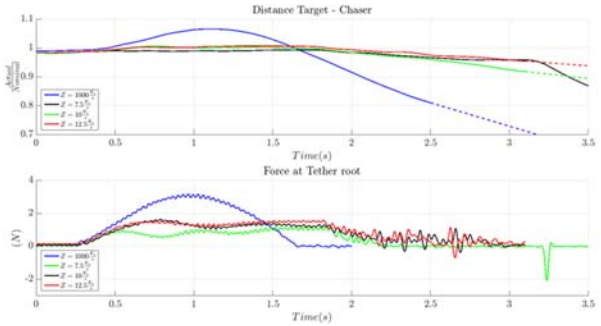

Figure 17 – Release Phase: relative distance and tether tension for different control impedances

In Figure 16 different stabilization test cases are presented for different tethers slack conditions. The blue line is the representation of the system without the effect of the WBC. Setting $Z = 1000$ kg s^{-1} meant no control, from a practical point of view: with this value, it was reasonable to neglect the effect of the WBC on the system dynamics, being at least one order of magnitude bigger than the estimated optimal *Z* values for the considered tethers. On the contrary, $Z = 10$ kg s^{-1} was selected to obtain the required performances by the controller (as explained in section 2 of this paper). With different slack conditions, the controller is still able to absorb the vibrations and leads to a considerable reduction of shock loads. Moreover, the frequency is higher but almost instantaneously damped. It is worth noticing how the WBC allows to obtain a constant tensioning of the tether at the end of the manoeuvre: the force measured by the load cell shows that no collapsing of the tether occurs when a suitable parameter *Z* for the controller is selected (the collapse is evident instead in the case without control).

In Figure 17, the effectiveness of the controller during the release phase, i.e. at the end of the pulling phase, is analysed for different controller gains *Z*. The controller was able to damp the residual energy at the end of the pulling and the final relative velocity between chaser and target was decreased allowing to reach a stable quasi-constant (see perturbations due to g-jitter) relative distance. The robustness of the controller was verified

by setting Z as 25% higher or lower than the nominal value: it is possible to remark how the control performance were preserved even with values of *Z* far from the optimal value. Such result is very important orbital operations, where uncertainties on tether and target parameters would not affect the successful outcome thank to the intrinsic robustness of the WBC.

4 CONCLUSIONS

Space tethered-tugs are a promising technology for future space transportation and active debris removal in Earth orbits. At PoliMi-DAER, a multibody simulation tool to describe the tethered dynamics was implemented, in order to design the system from both structural and GNC points of view. A wave-based controller was also implemented and simulated and was found to have good performances and robustness.

In order to validate the adopted multibody models and test their control laws, an experiment was selected to fly on board a parabolic flight campaign in October 2016, in the framework of the ESA Education Programme Fly Your Thesis! 2016. A scaled floating breadboard was tested in microgravity and its dynamics was reconstructed through stereovision and acceleration sensors. The SatLeash experiment demonstrated the possibility of using tow-tethers for space transportation. In particular, this experiment, being the first of its kind, represented an important milestone in the development of tethers for space transportation.

The experiment successfully demonstrated the capabilities of the developed wave-based control law. Good results were obtained in terms of performances and robustness. In fact, the instability effects were strongly mitigated and the advantageous control effects are present even with values of the control parameter far from the nominal one. This indicates a considerable robustness to uncertainties of the proposed control approach and suggest the possible exploitation of these control methods for orbital applications. The full dataset processing and model validation is still a work on-going.

Finally, an illustrative video[2] was recently published on YouTube by ESA Education, where the interested reader can watch both the experiment preparation and integration inside the airplane as well as some shots of the parabolic flight itself. The team is also planning a new campaign to test other controllers and be able to carry out a comparative analysis as the one presented using the simulations output.

5 ACKNOWLEDGMENTS

The authors would like to acknowledge the European Space Agency Education Office for supporting this project and granting the parabolic flight facility. The authors would also like to thank for their sponsorship FESTO who provided the actuation system and GOTTIFREDI-MAFFIOLI who provided the test ropes.

[2] https://www.youtube.com/watch?v=KDULeDX_ulM

6 REFERENCES

1. Liou J.C. and Johnson N.L., "*A sensitivity study of the effectiveness of active debris removal in LEO*", 58th International Astronautical Congress, Hyderabad, India, 2007.

2. Bastida B. and Krag H., "*Analyzing the criteria for a stable environment*", AAS/AIAA Astrodynamics Specialist Conference, Girdwood, Alaska, 2011.

3. Aslanov V. and Yudintsev Y., "*Dynamics of large debris connected to space tug by a tether*", Journal of Guidance, Control and Dynamics, 2013.

4. Aslanov V. and Yudintsev Y., "*Dynamics of large space debris removal using tethered space tug*", Acta Astronautica, 2013.

5. Jasper L. and Schaub H., "*Input shaped large thrust manoeuvre with a tethered debris object*", 6th European Conference on Space Debris, ESOC, Darmstadt, Germany, April 2013.

6. Jasper L. and Schaub H., "*Discretized input shaping for a large thrust tethered debris object*", AAS/AIAA Space Flight Mechanics Meeting, Santa Fe, NM, January 2014.

7. Leamy M.J., Noor A.K. and Wasfy T.M., "*Dynamic simulation of a tethered satellite system using finite elements and fuzzy sets*", Comput. Methods Appl. Mech. Eng, 2001.

8. Williams P., "*Dynamic multi-body modelling for tethered space elevators*", Delft University of Technology, March 2009.

9. Benvenuto R. and Lavagna M., "*GNC techniques for proximity manoeuvring with uncooperative space objects*", 6th International Conference on Astrodynamics Tools and Techniques, Darmstadt, Germany, March 2016.

10. Benvenuto R., Lavagna M. and Salvi S., "*Multibody dynamics driving GNC and system design in tethered-nets for active debris removal*", Advances in Space Research, Vol. 58, Issue 1, July 2016.

11. Benvenuto R. and Lavagna M., "Towing Tethers to Control Debris Removal Dynamics", 65th

International Astronautical Congress (IAC), Toronto, Canada, October 2014.

12. da Cruz Pacheco G.F., Carpentier B. and Petit N., "*De-orbiting of space debris by means of a towing cable and a single thruster spaceship: whiplash and tail wagging effects*", 6th European Conference on Space Debris, Darmstadt, Germany, April 2013.

13. O'Connor W. J., Cleary S. and Hayden J. D., "*Debris de-tumbling and de-orbiting by elastic tether and wave-based control*", 6th International Conference on Astrodynamics Tools and Techniques (ICATT), Darmstadt, Germany, March 2016.